Sensors & Diagnostics

PAPER

View Article Online
View Journal | View Issue

Cite this: *Sens. Diagn.*, 2024, **3**, 309

Rapid test for platelet viability relying on a quartz crystal microbalance assay†

Felix Thier[ab] and Peter A. Lieberzeit *[a]

Sensing systems provide a fast and cost-effective way to monitor health parameters and can thus help medical personnel to ensure optimal care for patients. In this study, we present a sensor based on quartz crystal microbalances (QCMs) with bare, non-modified gold electrodes to monitor viability of platelets in stored platelet concentrates used in transfusion medicine. The system is useful to determine cell viability both in static and continuous flow experiments. Sensor responses correlate with platelet viability: viable cells have the ability to activate and aggregate and, thus, firmly attach to the QCM gold surface, in turn causing high frequency shifts due to a change in viscoelastic properties. For instance, on the fifth day of storage, platelet samples led to QCM frequency shifts less than 40% of the signal obtained from the fresh concentrate. Sensor results correlate well with a resazurin-based fluorescence viability assay. This also correlates with optical and atomic force microscopy (AFM) images that reveal changes in platelet morphology during the storage period, namely cessation of extensive pseudopodia formation and platelet spreading. Platelet size in solution significantly increased during storage, most likely due to a pH drop in the medium. The straightforward system is thus in principle useful to detect storage lesions and viability of platelets directly before transfusion.

Received 10th October 2023,
Accepted 20th December 2023

DOI: 10.1039/d3sd00269a

rsc.li/sensors

Introduction

State-of-the-art medicine relies on precise and fast analyses to ensure ideal treatment for patients. For instance, monitoring blood parameters and the quality of blood products in real time is crucial in many settings.[1] Observing platelet count and function, for instance, is necessary when treating patients suffering from platelet disorders,[2] but also in hospitals, during surgery, and in ICUs.[3,4] When the platelet count falls below a certain threshold or platelet function is impaired, doctors need to administer platelet concentrates.[5,6] Herein, we describe a cost-effective and rapid method to monitor the quality of platelet concentrates relying on quartz crystal microbalances (QCMs).

Platelets, or thrombocytes, are the smallest cellular blood components. The anucleate, discoid fragments originate from megakaryocytes mainly in bone marrow and have a mean diameter between 2–4 μm.[7] Platelets circulate in the blood stream in a resting state for 7–10 days, until macrophages remove them.[8] The normal platelet count in a healthy adult ranges from approx. 150 000 to 400 000 cells per μL blood.[9] Platelets play a key role in haemostasis, but also in inflammatory regulation and wound healing.[8] Haemostasis (coagulation) can be divided into two steps: primary haemostasis is the first response towards an injured blood vessel. After vasoconstriction, inactive, circulating platelets adhere to the protein von Willebrand factor (VWF) on the exposed subendothelial collagen, thus activating platelets. They then change their shape *via* extensive pseudopodia formation (re-arrangement of cytoskeleton) and spreading (attached cells widen their contact area *via* plasma membrane deformation),[10] which in turn leads to exocytosis of intracellular granules. They thereby release a range of compounds (*i.e.* thromboxane A2, adenosine diphosphate and serotonin) that further promote conformational changes in platelets and pronounced vasoconstriction of the surrounding blood vessels. Furthermore, it promotes binding to fibrinogen, leading to platelet aggregation.[11] This so-called "white thrombus" is the primary plug to prevent further blood loss. Secondary haemostasis then comprises the formation of a hard thrombus, where a crosslinked, insoluble fibrin mesh forms around the platelet plug. The serine protease thrombin is responsible for transforming soluble fibrinogen to the stabilizing fibrin mesh, forming the solid blood clot.[7,11]

Thrombocytopenia describes the condition when the platelet count in the blood stream is too low, while

[a] *Faculty of Chemistry, Department of Physical Chemistry, University of Vienna, Währinger Str. 42, 1090 Vienna, Austria. E-mail: Peter.Lieberzeit@univie.ac.at*
[b] *Vienna Doctoral School in Chemistry (DoSChem), University of Vienna, Währinger Str. 42, 1090 Vienna, Austria*

† Electronic supplementary information (ESI) available. See DOI: https://doi.org/10.1039/d3sd00269a

thrombocytopathy means impaired platelet function, *i.e.* coagulant activity.[12] Both events may require transfusion of platelet concentrates to prevent haemorrhagic incidents. Additionally, injuries with high blood loss and high dose chemotherapy may require supportive platelet transfusion.[13] Transfusion medicine thus requires platelet concentrates.[14] Those commonly consist of a mixture of plasma and platelet additive solutions (PAS) and contain from 2 to 8 × 10^{11} platelets per unit.[13,15] Administration of one unit is expected to elevate platelet count by 30 000–50 000 platelets per μL.[14] The usual shelf life of a platelet concentrate is 5 days. Pathogen inactivation may extend the period to 7 days.[13]

Typical methods to analyse platelet count and function range from simple ones such as bleeding time measurements to more elaborated ones such as light transmission aggregometry.[16] While the simple methods (*i.e.* bleeding time) are poorly standardised and often suffer from the influence of the person carrying out the analysis,[17] elaborated methods may rely on costly devices and in some cases suffer from long analysis time.[4] Usually, the measuring time is inversely proportional to the ability of the platelets to aggregate, *i.e.*, the less they do (and: the more urgently a patient needs treatment), the longer they take. Furthermore, there is a strong drive to making medicine less invasive, which in the case of blood testing means reducing the sample volumes as much as possible. Therefore, it is of inherent interest to design methods that are suitable for implementing in microfluidic environments. This is also fundamentally interesting for determining the quality and/or viability of platelet concentrates, which are a valuable commodity.

The past two decades have seen some studies using QCMs to monitor platelet function and study platelet behaviour.[18–28] The present work, however, comprises the first approach to monitor platelet viability directly in a platelet concentrate and thereby to assess the quality of platelet concentrates prior to possible administration.

The QCM is a small, mass-sensitive quartz resonator: its resonance frequency is proportional to mass load as described by G. Sauerbrey in 1959.[29] When measuring in the liquid phase, the frequency shift additionally depends on the viscoelastic properties of both the solution and the analyte layer itself as described by the so-called Kanazawa–Gordon equation.[30–34] In this study, we use changes in platelet properties upon storage to measure their viability using the QCM in comparably small sample volumes, namely around 150 μL.

Platelet storage lesion is the umbrella term for events occurring during storage (*e.g.* storage-induced activation,[35] surface receptor modifications[36] and morphological changes[37]), negatively affecting platelet viability and therefore concentrate shelf life and efficacy. They take place due to alterations in platelet metabolism *in vitro* and due to storage-induced stress,[8] as well as possible bacterial contamination.[36] Quality assessment usually comprises determining the platelet count and the number of remaining white blood cells directly after production. Sterility testing usually takes place close to the end of shelf life. Thus, the only quality assessment directly before administration of a platelet concentrate to a patient takes place visually by approving the presence of swirling.[38] Herein, we suggest a non-biased, rapid, and facile testing system to replace that rather inexact approach.

Experimental

Materials and reagents

Sodium chloride was purchased from AppliChem. Hydrochloric acid, magnesium chloride hexahydrate, potassium dihydrogen phosphate, di-sodium hydrogen phosphate dihydrate and sodium hydroxide were supplied by Merck. Sodium hydrogen carbonate was obtained from abcr. HEPES was purchased from Alfa Aesar and potassium chloride was supplied by VWR chemicals. Sodium dodecyl sulfate (SDS) was purchased from Chemsolute. All chemicals were used without further purification. Calcium- and albumin-free Tyrode's buffer (pH 7.4) was prepared in-house and consisted of 134 mM NaCl, 12 mM $NaHCO_3$, 2.9 mM KCl, 0.34 mM $Na_2HPO_4 \times 2H_2O$, 1 mM $MgCl_2$ and 10 mM HEPES.

Platelet sample treatment

Aliquots of blood-type specific, pooled human platelet concentrates were obtained from the Austrian Red Cross Blood Donation Centre Vienna prior to pathogen reduction. Platelet samples were collected in EDTA-buffered test tubes (Sarstedt S-Monovette® EDTA KE) with a maximum volume of 4.9 mL and stored at adequate conditions, meaning room temperature (22 ± 2 °C), darkness, and constant, smooth agitation. On selected days during the storage period of up to 11 days (*i.e.* on day 1–5, 8 and 11), a 1 : 10 dilution of the original platelet sample in modified Tyrode's buffer was prepared and purified *via* a centrifugation step (7 min, 2300 rpm/800 RCF) to reduce plasma protein content. The resulting supernatant was discarded, and the platelet pellet was then resuspended in phosphate-buffered saline (PBS; 1×, pH 7.4). Sensor measurements of the purified platelet samples were carried out in triplicates, each having a total volume of 1 mL. Cell counting of samples took place on a cell counter (CASY Cell Counter with 45 μm capillary, OMNI Life Science GmbH & Co KG) prior to QCM measurements at room temperature in CASYton, a physiological background buffer.

In addition to the cell count, we determined mean platelet diameter and volume changes during storage using the CASY cell counter.

Fabrication of quartz crystal microbalances

Quartz crystal microbalances (QCMs) were fabricated in-house on 10 MHz, AT-cut quartz disks with a diameter of 13.8 mm purchased from Roditi International Corporation. Two backside electrodes with a diameter of 4 mm each were

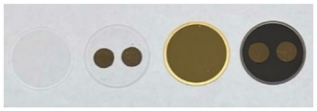

Fig. 1 From left to right: blank QCM chip, QCM chip with screen-printed contact electrodes, front- and backside of the ready-to-use QCM chip equipped with a fully metallized top electrode coated *via* PVD and the screen-printed bottom electrodes.

screen-printed onto the quartz surface using 10% brilliant gold paste (GGP 1229 DH, Heraeus). We coated the sample side of the blank quartz disks by physical vapor deposition (PVD), involving magnetron-sputtering of 8 nm Ti and thermal evaporation of 50 nm Au (HEX deposition system, Korvus Technology) to fully metallize the surface. Fig. 1 depicts a blank QCM chip and QCM chips coated with the respective electrode structures. The "backside" electrodes were connected to the respective oscillator circuit, whereas the fully metallized surface was electrically grounded. We used the dual-electrode design to compensate for fluctuations in physical parameters (*i.e.* temperature and viscosity), as already described in ref. 39. The setup additionally accounts for enhanced reproducibility and accuracy, as each electrode allows for performing an individual measurement, *i.e.* two per QCM.

QCM sensor measurements

Prior to each sensor measurement, QCMs were cleaned with ethanol and acetone and treated with oxidative plasma at a pressure of 1.3×10^{-3} mbar and a power of 5.5 W for 5 min (Zepto One, Diener). QCMs were then placed in the flow cell and connected to the oscillator circuit. Each measurement was carried out at room temperature in a horizontal setup using PBS as the background buffer. After reaching stable signal baseline, we exposed the QCMs to the respective platelet sample by injecting 500 μL of the purified, 1 : 10-diluted platelet concentrate in PBS into the flow cell and allowing the platelets to sediment on the bare QCM gold surface for at least 20 min. After that, we flushed the system three times with PBS and two times with water. Signal read-out took place prior to flushing (*i.e.* after 20 min of sedimentation) and comprised a mean of up to 6 sensor responses per day. We carried out daily measurements simultaneously to minimize time-dependent signal alterations.

To simulate real-life platelet transfusion conditions and venous blood flow, we additionally carried out sensor measurements at constant flow conditions. We connected the QCM flow cell tubes to a peristaltic pump and allowed the QCM to reach baseline signal in PBS at a constant flow of 1 mL min^{-1}. We then introduced the samples by placing the tubes into a solution containing $3–9 \times 10^4$ platelets per mL in PBS (total volume: 5 mL). The flow was kept constant at 1 mL min^{-1} for a measurement time of 20 min. After 10 min, the flow direction was reversed to ensure even distribution of the platelets in the measurement cell. Platelet samples were steadily pumped through the flow cell by placing the outlet tube in the same container as the inlet tube. After introducing the platelets, we flushed 5 min with PBS. After measurement, the QCMs were rinsed with water for 2 min directly in the flow cell. We measured one sensor response per day per sample for a total of 4 days.

Platelets were removed from QCM surfaces after sensor measurements by incubating them in a solution containing 5% SDS in 0.1 M NaOH directly in the flow cell. Removing the QCM from the flow cell additionally allowed for applying organic solvents (ethanol and acetone) and mechanical force with a microfibre cloth. The pieces of cloth were soaked with the respective solvent and gently wiped over the QCM surface to remove adhered platelets and fully clean gold surfaces.

Optical and atomic force microscopy

After QCM measurements, the morphology of remaining, sedimented platelets on the sensor surface was assessed using optical microscopy (ECLIPSE LV100, Nikon) and atomic force microscopy (AFM; MultiMode 8, Bruker). We operated the AFM in tapping mode in air using Scout 350 RAl probes (NuNano). QCM surfaces were scanned directly after sensor measurements without additional sample preparation. The open-source software Gwyddion served for data evaluation and image processing. If necessary, image curvature was flattened using polynomial background subtraction; horizontal scars were removed using the built-in algorithm.

Fluorescence viability assay

To validate sensor results, we assessed platelet viability using a resazurin fluorescence assay. Here, resazurin is reduced to resorufin by reductases in metabolically active cells, allowing conclusions on cell viability[40] (Fig. 2).

Aliquots (490 μL) of the samples used for QCM measurements were incubated with 20 μL of CellTiter-Blue® (Promega) resazurin dye for 2 h at 37 °C in the dark. After incubation, platelet samples were centrifuged at 4400 rpm/3000

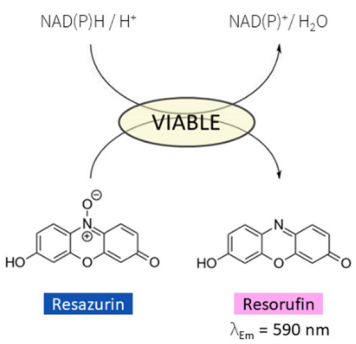

Fig. 2 Scheme of resazurin reduction to fluorescent resorufin by reductases in metabolically active cells using NADH or NADPH. Observing fluorescence emission at 590 nm allows conclusions on cell viability.

RCF for 10 min, ensuring complete pelleting of the cells. We then collected 400 μL of the remaining supernatant for fluorescence assay and immediately froze the samples at −20 °C until further use. Additionally, one blank sample per day was created (490 μL PBS and 20 μL dye) and treated equally as the platelet samples. Prior to spectral collection, samples were thawed and diluted 1 : 30 with PBS. Fluorescence emission spectra were then collected using the LS 55 fluorescence spectrometer (PerkinElmer) with constant λ_{Ex} = 560 nm and λ_{Em} = 570–650 nm. Spectra were acquired using a scanning speed of 40 nm min^{-1}. Fluorescence intensity was read out at λ_{Em} = 590 nm. Finally, inherent background fluorescence was removed by subtracting the mean value of the blank samples at λ_{Em} = 590 nm; all fluorescence intensities were normalized to a platelet count of 10^7 cells per mL.

Results and discussion

QCM sensor results

Fig. 3 shows the QCM frequency shifts of a fresh (A) and an old (B) platelet sample measured at physiological concentrations (*i.e.* 10^5 platelets per μL) in modified Tyrode's buffer (pH 7.4). We measured the fresh sample aliquot after one day of storage and the old sample aliquot several weeks after obtaining it. By that time, one can conclude that the platelets have undergone apoptosis and, thus, show zero metabolic activity. The results in this first measurement in Fig. 3 show that the signal output (*i.e.* frequency shift) strongly varies between fresh and old platelet samples, namely by an order of magnitude.

One can directly link this to their ability to aggregate: sedimentation and contact with the QCM gold surface triggers the activation mechanism in metabolically active platelets. Hence, cells spread and aggregate and thereby firmly attach to the QCM surface. This changes the viscoelastic properties and increases the binding strength of platelets to the surface and, thus, causes a higher frequency shift compared to aged cells. The latter lack the ability to aggregate for the lack of active metabolism. Therefore, they bind to the QCM electrode to a lower extent, leading to smaller frequency shifts. Naturally, it is thus possible to assess viability of the cells, which requires metabolic activity.

This finding allows for establishing a sensor approach to monitor viability in platelet concentrates. Fig. 4 shows sensor responses of purified platelet concentrates measured at sub-physiological concentrations (*i.e.* 2–7 × 10^4 platelets per μL). Sensor responses were read out after 20 min. The data shown in Fig. 4 indicates strong decrease in frequency shifts depending on the storage time of platelet concentrates, correlating with the findings presented in Fig. 3. Again, the platelet sample causes higher frequency shifts at the beginning of the storage period at roughly −170 Hz. The sensor signals then decrease steadily until reaching around −30 Hz on the last day of storage. Table 1 summarizes the observed frequency shifts. The high standard deviations at day 2 and day 4 can be traced back to high plasma protein content: in some of the samples, it turned out impossible to remove it by centrifugation.

Fig. 5 shows AFM images of a QCM measured on day 2 after termination of the sensor measurement and flushing with PBS and water. Clearly, branches of agglomerated proteins are visible in the image recorded at a scan size of 50 × 50 μm. Decreasing the scan size to 1 × 1 μm supposedly

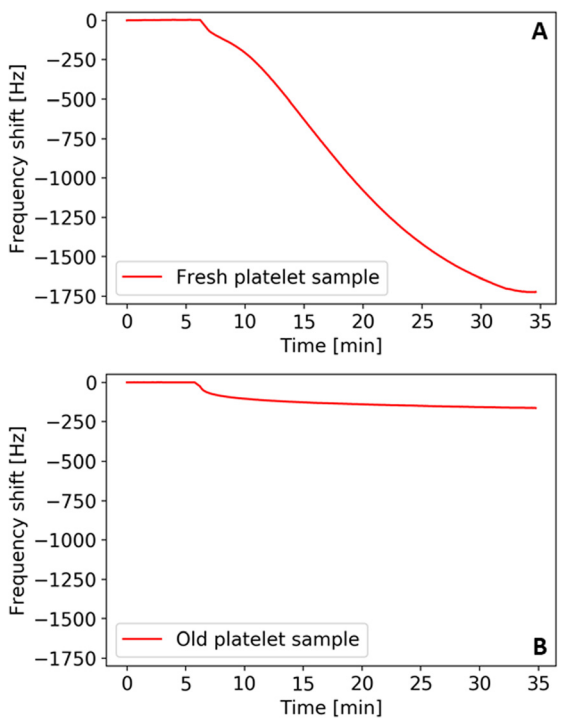

Fig. 3 QCM frequency shifts of a platelet sample stored for one day (A) and ten weeks (B), recorded at physiological concentrations in modified Tyrode's buffer (pH 7.4). Adherence to the QCM gold surface can be regarded a function of cell viability.

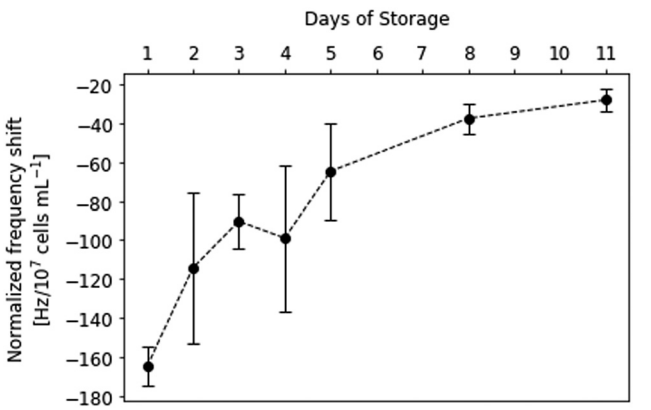

Fig. 4 Normalized QCM frequency shifts recorded at sub-physiological platelet concentrations (2–7 × 10^4 platelets per μL) of a platelet concentrate stored throughout 11 days. Frequency shifts were read-out after 20 min of sedimentation under static conditions in PBS buffer (pH 7.4) and show a constant decrease throughout the storage period (n = 2–6 sensor responses per day, error bars represent standard deviations).

Table 1 Measured normalized frequency shift of platelet concentrate stored for 1 to 11 days

Day of storage	Normalized frequency shift [Hz/10^7 cells per mL]
1	−165 ± 10
2	−114 ± 39
3	−90 ± 14
4	−100 ± 38
5	−65 ± 25
8	−38 ± 8
11	−28 ± 6

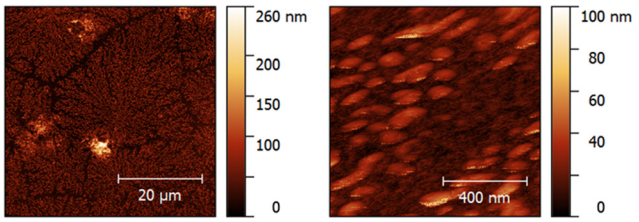

Fig. 5 AFM images of a QCM sensor surface after measuring the platelet concentrate sample at the 2nd day of storage. Left: 50 × 50 µm scan size reveals branches of agglomerated proteins surrounding attached platelets. Right: 1 × 1 µm scan size shows protein aggregates with a major diameter of 137 ± 10 nm, a minor diameter of 63 ± 8 nm and a height of 31 ± 4 nm (n = 6).

reveals spherical to ellipsoidal protein clusters with a major diameter of 137 ± 10 nm and a minor diameter of 63 ± 8 nm. The protein agglomerates are 31 ± 4 nm (n = 6) high. Human serum albumin (HSA), the most abundant plasma protein in the human body, most likely accounts for the visible agglomerates, together with other plasma proteins such as fibrinogen. The protein layer additionally increases the mass load on the QCM surface and, therefore, causes higher frequency shifts. Additionally, platelets might adhere to the protein layer more readily than to the bare gold surface,[41,42] leading to more platelets firmly attaching to the active electrode area. Those two factors cause higher frequency shifts than expected in some of the sensor measurements. Therefore, one can assume that they account for the comparably high standard deviations observed on day 2 and day 4 (Fig. 4). Thus, it is necessary to improve the centrifugation step for future measurements. If feasible, it should be replaced by filtration. Nonetheless, the results demonstrate that it is possible to measure platelet viability directly with the QCM: signals steadily decrease depending on storage time. Furthermore, it is not necessary to apply any sensitive layer on the QCM electrode to measure platelet viability in purified concentrates, thus underlining the ease of use of the system. The system in principle is sufficiently rugged for everyday use. Of course, one has to ensure constant temperature during measurements, but external interferences such as mechanical vibrations do not alter the frequency characteristics of the sensors used (see ESI†).

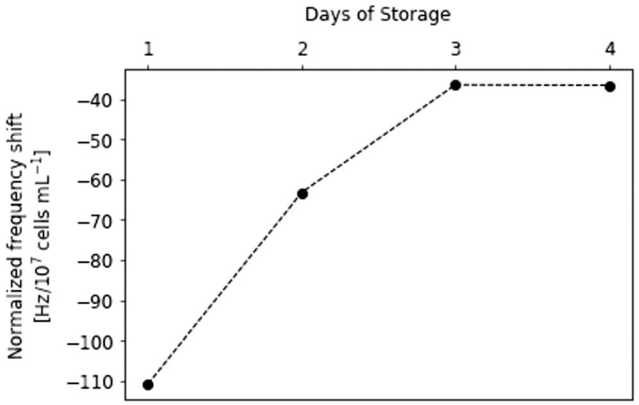

Fig. 6 Normalized QCM frequency shifts recorded at sub-physiological platelet concentrations (4–10 × 10^4 platelets per µL) in continuous flow (flow rate: 1 mL min^{-1}) in PBS buffer.

Continuous flow conditions

Fig. 6 shows QCM results obtained in continuous flow for a platelet concentrate stored for 4 days. Platelet transfusions are usually carried out at a flow rate of 2–5 mL min^{-1} or less in patients with the risk of fluid overload.[43] Naturally, observing platelet viability prior to transfusion is more important for patients at risk, which is why a flow rate of 1 mL min^{-1} was chosen for this experiment measuring only one sensor response per day.

Continuous flow results in fewer platelets sedimenting on the gold electrode. This leads to slightly smaller frequency shifts on the sensor compared to static sedimentation: on the first day it was −111 Hz; on the second day −63 Hz after 20 min of platelet flow. On day 3, the frequency shift was −37 Hz, which did not significantly change at the fourth day of storage. Hence, signals in continuous flow experiment are approx. 33 to 63% lower than during static sedimentation measurements, respectively, from day 1 to day 4. The results of the two experiments, however, are consistent: clearly, frequency shifts rapidly decline between day 1 and 3, with no further significant change on day 4. This means that after three days storage most platelets seem no longer metabolically active. Apparently, most of the important processes of platelet storage lesion happen between day 1 and day 3.

Morphological characterisation of platelets

Platelets undergo morphological changes upon activation and aggregation (*i.e.*, pseudopodia formation and spreading on the surface). The optical microscopy images in Fig. 7 highlight them during the storing period. Images were collected directly after the respective QCM measurements. Clearly, cell shapes differ throughout the images. Upon contact with the gold electrode, metabolically active platelets start forming pseudopodia, as shown in the image collected at day 1. Pseudopodia are also visible to a large extent in day 2 platelets, but their number decreases in images taken on day 3 and day 4. From then on, the cells form increasingly

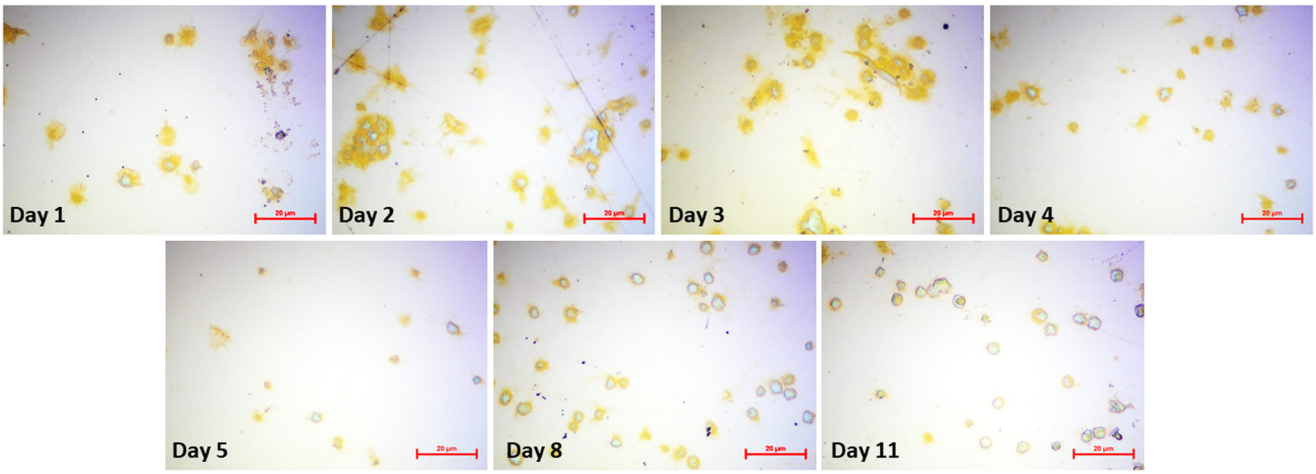

Fig. 7 Optical microscopy images of sensor surfaces after QCM measurements. Surfaces were flushed with PBS and water prior to microscopy to remove any unbound cells. (Bars: 20 μm).

fewer pseudopodia. At the 11th day of storage, the process stops. This finding does not only affirm the observed QCM frequency shifts, but also agrees with average platelet lifespan in general (*i.e.* 7–10 days). Platelet spreading also clearly decreases in a similar manner: viable platelets maximize their contact areas on the gold surface by rearranging their plasma membrane to a flat disk. Again, this effect is strongest on day 1, but also visible on images taken on day 2, day 3, and, to some extent, on day 4. Starting from day 5, platelet spreading becomes rare and completely disappears in platelets stored for 11 days. Hence, viability as a measure of spreading is also directly correlated to sensor responses.

The appearance of platelet aggregates is another important feature observable in optical microscopy. Naturally, viable platelets tend to aggregate more easily than non-viable ones, because platelet aggregation is an important step for thrombus formation and blood coagulation. Thus, more aggregates can be seen in images taken at day 1–4 compared to images taken at the end of the storage period. Here, individual platelets are present on the QCM surface.

AFM images (Fig. 8) confirm this trend. The platelet on the 1st day of storage clearly shows all signs of prior active metabolism: pseudopodia are surrounded by a spread plasma membrane. The cell in the image recorded at day 2 also shows slight pseudopodia formation and spreading. This image additionally shows protein clusters, represented as small bright dots surrounding the spread platelets. Spreading and pseudopodia formation is no longer visible in the images scanned on day 4 and day 8, respectively. Here, platelets have preserved their discoid shape. The cell recorded in the lower half of the AFM image at day 4 resembles a ghost cell, most likely resulting from a dead platelet.

The microscopy images in Fig. 7 help explaining QCM data in Fig. 4 and Table 1: not only the frequency shifts caused by adsorption of the platelets decrease with storage time, but also the absolute and relative errors of frequency shifts. In fact, signals of uncoated QCMs comprising several electrodes (two, in our case) should not differ by as much as a third; this is substantially higher than one would expect for smooth, PVD-deposited electrodes and hints at uneven distribution of platelets on the device surface. That is indeed the case, as one can see in Fig. 7. From the measuring perspective, this first looks like a drawback: it is well-known that the sensitivity of QCM electrodes is highest in the centre and decreases to zero towards the edges.[44] Even though all measurements in that regard took place in the gas phase, it is valid to assume similar effects in liquids. However, it is possible to use a QCM comprising several electrode pairs to obtain both frequency shifts and their confidence intervals during one measurement. For instance, it is possible to include up to four electrode pairs on a 10 MHz QCM.[45] In the same way, this also compensates for effects of varying temperature: in liquids, this leads to fluctuations in viscosity, which strongly influence the frequency shift as described by the Kanazawa–Gordon equation.

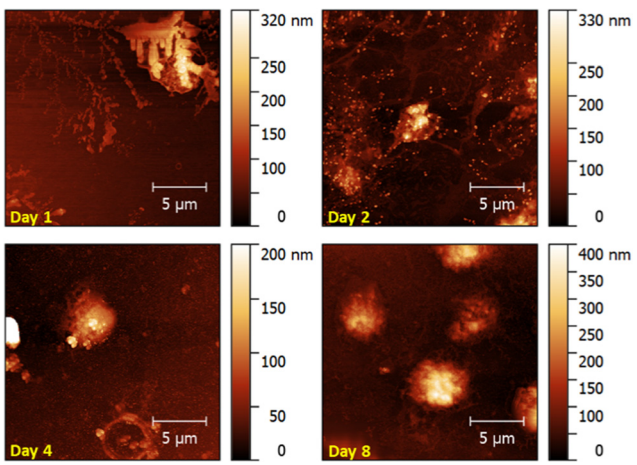

Fig. 8 AFM images of QCM surfaces after sensor measurements (scan size: 20 × 20 μm).

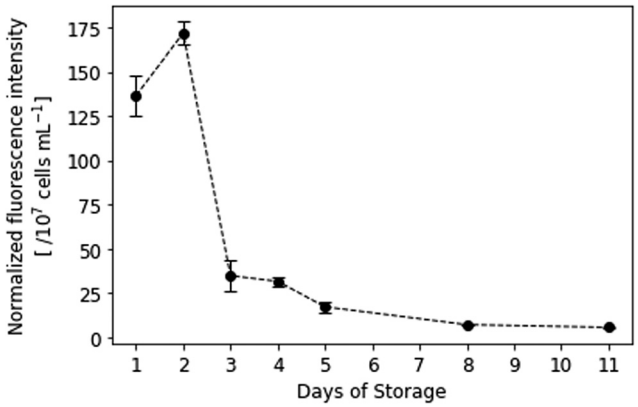

Fig. 9 Normalized fluorescence intensity of resazurin-dyed platelet samples. λ_{Ex} = 560 nm, λ_{Em} = 590 nm. Spectral collection was achieved in PBS at room temperature (n = 3).

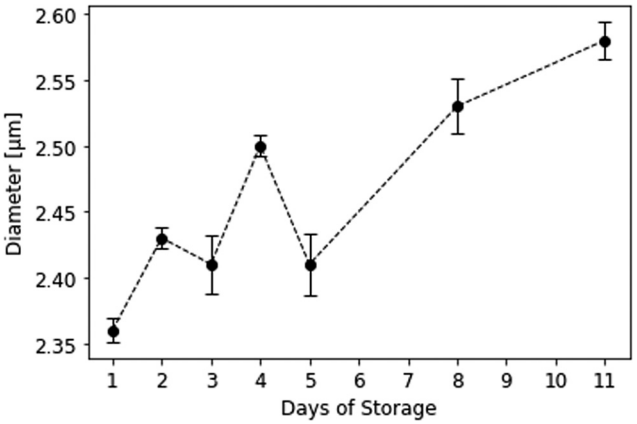

Fig. 10 Mean platelet diameters in solution during storage measured at the CASY cell counter. Background buffer was isotonic CASYton at room temperature (n = 3).

Platelet viability assessed with fluorescence assay

Fluorescence data of the resazurin viability assay (Fig. 9) additionally underlines the QCM measurements: during the first two days of storage, platelets still exhibit high metabolic activity. A paired, two-tailed t-test revealed that those differences (*i.e.* between days 1 and 2) are not statistically significant (p = 0.038, where difference was significant if $p <$ 0.01). Fluorescence intensity then rapidly declines on day 3, which agrees with the QCM frequency shifts presented in Fig. 4 and 6. Only viable cells can convert resazurin to fluorescent resorufin, while dead cells do not. Thus, standard deviations are lower than in QCM measurements, because the amount of protein present in the sample does not affect the fluorescence signal. However, resazurin staining is affected by multiple factors, such as incubation time, distribution of the dye in the sample matrix and cell concentration,[40] which might explain the higher fluorescence intensity observed at day 2.

Morphological platelet changes in solution

Interestingly, mean platelet diameters in solution significantly increased during storage, especially between the 5th and the 11th day. More dead cells lead to a shift in mean platelet diameter to larger values. This can be traced back to a supposed pH drop in stored platelet concentrate and the resulting disk-to-sphere transition of platelets.‡ During storage, platelets consume glucose and produce lactate.[46] The latter causes pH to drop, causing platelets to swell and morphologically change from disk to sphere. This results in larger cell volumes (and thus, larger diameters) measured on the CASY cell counter. Initial mean platelet diameters were 2.36 ± 0.01 µm on the first day and changed to 2.58 ± 0.01 µm on the 11th day of storage (Fig. 10). Mean platelet volumes ranged from 7.644 ± 0.068 fL on day 1 to 9.893 ± 0.129 fL on day 11. Table 2 summarises platelet diameters and volumes during storage. Swelling of platelets and their morphological change in solution additionally correlates with our QCM sensor measurements: viable, discoid shaped cells with small mean diameters strongly adhere to the QCM surface, while spherical, dead cells only loosely attach to the gold electrode, leading to lower signals.

Regenerating QCM sensors after measuring

In the light of commercially applying the sensor system, it is highly desirable that one can reuse the QCM after measuring. Therefore, it is necessary to remove bound platelets from the gold surface. This is possible directly in the flow cell by flushing and incubating the system with a 0.1 M NaOH solution containing 5% SDS after the viability assay. Being a surfactant, SDS can disrupt and solubilise cell membranes.[47] In addition, the alkaline pH denatures proteins. The solution thus detaches platelets from the gold surfaces. We tested this on a "worst-case scenario", *i.e.* QCM stored for more than 9 months after carrying out the viability assay. Logically, platelet cells on the gold surface are completely dried after that period. Nonetheless, it is possible to remove them: Fig. 11 shows optical microscopy images of the QCM chip before (A) and after (B) incubating it for one hour in NaOH/

Table 2 Mean platelet diameters and volumes during the storage period of 11 days

Day of storage	Diameter [µm]	Volume [fL]
1	2.36 ± 0.01	7.644 ± 0.07
2	2.43 ± 0.01	8.241 ± 0.06
3	2.41 ± 0.02	8.423 ± 0.18
4	2.50 ± 0.01	9.016 ± 0.05
5	2.41 ± 0.02	8.377 ± 0.22
8	2.53 ± 0.02	9.305 ± 0.16
11	2.58 ± 0.01	9.893 ± 0.13

‡ Due to the low sample volume available, the exact pH could not be measured with the means we had available in the laboratory during the time the research was conducted.

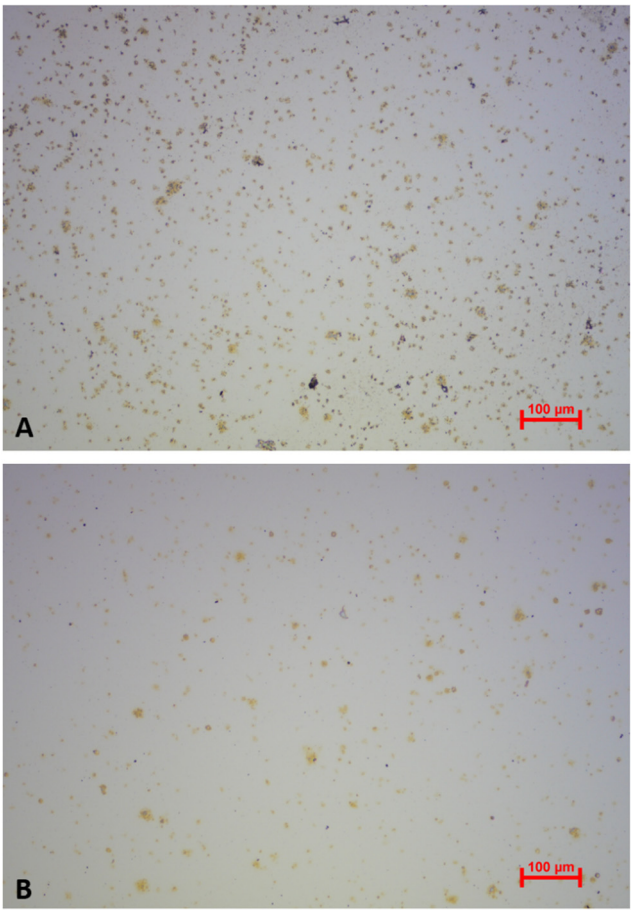

Fig. 11 Optical microscopy images (10-fold magnification) of a QCM chip with immobilised platelets before (A) and after (B) incubation with 0.1 M NaOH/5% SDS for 1 h directly in the QCM flow cell 9 months after viability measurement.

SDS directly in the QCM flow cell. Clearly, the surface after incubation (Fig. 11B) contains substantially fewer platelets than before (Fig. 11A), thus proving removal.

To assess the effect of incubating QCM chips with NaOH/SDS in a more quantitative manner, the respective frequency spectra were recorded with a network analyser (E5062A ENA Series, Agilent Technologies). Fig. 12 shows the corresponding damping spectra before and after incubating a QCM chip with NaOH/SDS for 17 h. Again, QCM chips were cleaned more than 9 months after performing the viability assay.

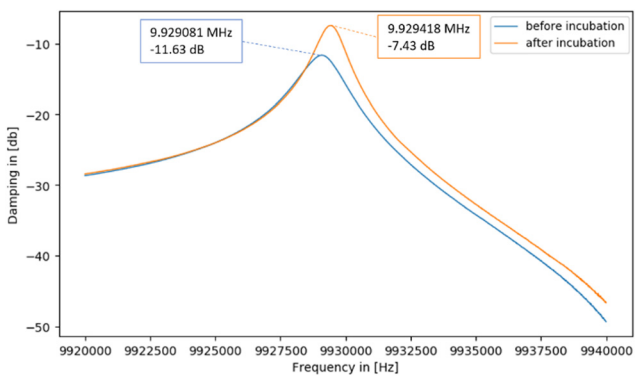

Fig. 12 Damping spectra of a QCM chip with immobilised platelets before and after incubating with 0.1 M NaOH/5% SDS for 17 h.

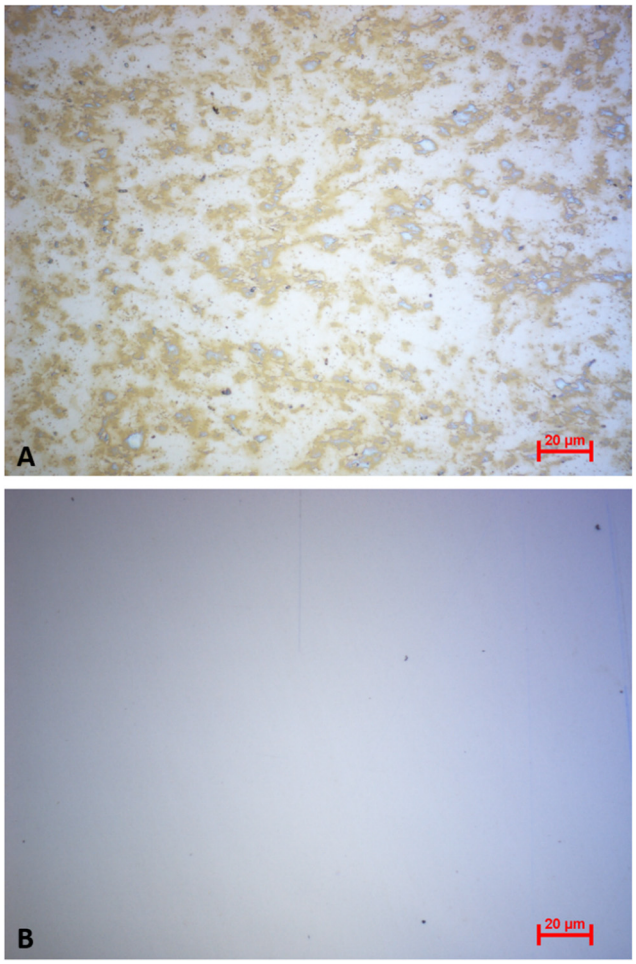

Fig. 13 Optical microscopy images (50-fold magnification) of a QCM surface immediately after platelet viability assay (A), and after chemical and mechanical cleaning using NaOH/SDS, ethanol, acetone and a microfibre cloth (B).

The spectra in Fig. 12 show that the resonance frequency increases by 337 Hz during incubation. This can be traced back to removing mass from its surface due to platelets detaching: the less mass on the QCM surface, the higher the resonant frequency. Also, the decrease in damping (from −11.63 dB to −7.43 dB) indicates successful removal: decreasing non-rigid mass loading of the sensor reduces damping.

It is also possible to remove platelets from the QCMs by applying organic solvents and (gentle) mechanical force. Fig. 13A shows an optical microscopy image of a QCM chip comprising platelets directly after the viability assay of a platelet concentrate stored for 2 days. Fig. 13B depicts the same QCM chip after applying a 0.05 M NaOH/1% SDS solution followed by mechanical cleaning using ethanol, acetone and a microfibre cloth 2.5 weeks after the viability

assay. Clearly, this completely removes platelets without significantly damaging the gold electrode of the QCM.

In the worst case, mechanically wiping gold electrodes may impair the quality of the gold surface, potentially reducing the number of cycles a QCM can undergo. Both mechanical and chemical techniques, however, are feasible for regenerating the device surface. They differ with respect to the time required: mechanical treatment is a matter of minutes, whereas incubation may last longer.

Conclusions

Platelet concentrates must fulfil certain criteria to be approved as acceptable for transfusion. This includes a sufficient platelet count (typically 2 to 8 × 10^{11} platelets per unit) and sufficient depletion of remaining white blood cells at the beginning of the storage period, as well as microbiological assessment towards the end of the shelf life. The only quality assessment directly before transfusion is visual inspection for the presence of swirling by medical staff. In this study, we provide a rapid and easy-to-use sensing system for monitoring platelet concentrate stability and quality. The system relies on bare-gold, non-functionalised quartz crystal microbalances, which can detect platelet viability *via* measuring their adhesive behaviour to the QCM gold surface. Fresh, healthy platelets at the beginning of the storage period cause high QCM frequency shifts. This is not the case for older, non-viable cells suffering from platelet storage lesion towards the end of the storage period. Upon sedimentation to the gold surface, viable cells are activated and therefore undergo extensive pseudopodia formation and spread over the surface. This in turn increases their adhesiveness to the surface due to a change in viscoelastic properties of the bound analytes, causing a significantly higher frequency shift compared to non-viable cells. Of course, dead cells do not trigger this activation mechanism anymore, because they are not metabolically active. Overall, this results in lower frequency shifts. Sensor results were similar when conducted at static and continuous flow of sample liquid: viable platelets from the fresh concentrate lead to higher frequency shifts compared to non-viable cells towards the end of the concentrate's storage period.

Fluorescence viability assay based on resazurin reduction to resorufin by metabolically active cells confirms the sensor results. Fluorescence data is consistent with QCM sensor responses, indicating a rapid decline of platelet viability at the third day of storage, followed by a consistent decrease until the last day of storage.

Morphological characterisation using optical and atomic force microscopy highlighted distinct events connected to platelet viability: in the beginning of the storage period (*i.e.* at day 1 to 4), one can observe significant pseudopodia formation and platelet spreading. Starting from day 5, those events become rare, indicating cessation of metabolism and thus viability. Morphological characterisation *via* cell counting in solution revealed that mean platelet diameter and volume increased during storage. This can be traced back to a drop in pH during storage and the resulting disk-to-sphere transition of the platelets.

The QCM sensing system presented in this study proved successful in determining viability of platelets directly in concentrates. This opens the way to develop a non-invasive, integrated sensing system for platelet function testing prior to platelet transfusion, ensuring optimal treatment for patients in need.

Author contributions

F. T.: conceptualization, methodology, software, investigation, validation, writing – original draft, visualization. P. A. L.: conceptualization, methodology, resources, writing – review & editing, supervision.

Conflicts of interest

There are no conflicts to declare.

Acknowledgements

We gratefully acknowledge the support of the Austrian Red Cross, especially Robert Geretschläger and the "special products unit" of the Blood Donation Centre Vienna. We are thankful for the supply with platelet samples and the answered questions during the project.

Notes and references

1 R. Bockholt, S. Paschke, L. Heubner, B. Ibarlucea, A. Laupp, Ž. Janićijević, S. Klinghammer, S. Balakin, M. F. Maitz, C. Werner, G. Cuniberti, L. Baraban and P. M. Spieth, *J. Clin. Med.*, 2022, **11**, 2408.
2 V. Palma-barqueros, N. Revilla, A. Sánchez, A. Z. Cánovas, A. Rodriguez-alén, A. Marín-quílez, J. R. González-porras, V. Vicente, M. L. Lozano, J. M. Bastida and J. Rivera, *Int. J. Mol. Sci.*, 2021, **22**, 1–32.
3 F. S. Neuenfeldt, M. A. Weigand and D. Fischer, *J. Clin. Med.*, 2021, **10**, 5369.
4 R. Paniccia, R. Priora, A. A. Liotta and R. Abbate, *Vasc. Health Risk Manage.*, 2015, **11**, 133–148.
5 F. Ferrer-Marin, S. Stanworth, C. Josephson and M. Sola-Visner, *Transfusion*, 2013, **53**, 2814–2821.
6 P. S. Alcaina, *J. Blood Med.*, 2020, **11**, 19–26.
7 P. E. J. van der Meijden and J. W. M. Heemskerk, *Nat. Rev. Cardiol.*, 2019, **16**, 166–179.
8 M. S. Y. Ng, J. P. Tung and J. F. Fraser, *Transfus. Med. Rev.*, 2018, **32**, 144–154.
9 E. C. Josefsson, W. Vainchenker and C. James, *Int. J. Mol. Sci.*, 2020, **21**, 1–12.
10 B. Furie and B. C. Furie, *N. Engl. J. Med.*, 2008, **359**, 938–949.
11 S. Pourshahrestani, N. A. Kadri, E. Zeimaran and M. R. Towler, *Biomater. Sci.*, 2019, **7**, 31–50.

12 G. Mohan, S. V. Malayala, P. Mehta and M. Balla, *Cureus*, 2020, **12**, 1–8.
13 A. Capraru, K. A. Jalowiec, C. Medri, M. Daskalakis, S. S. Zeerleder and B. M. Taleghani, *J. Clin. Med.*, 2021, **10**, 1990.
14 E. K. Storch, B. S. Custer, M. R. Jacobs, J. E. Menitove and P. D. Mintz, *Blood Rev.*, 2019, **38**, 100593.
15 H. Gulliksson, *Vox Sang.*, 2014, **107**, 205–212.
16 J. Le Blanc, F. Mullier, C. Vayne and M. Lordkipanidzé, *J. Clin. Med.*, 2020, **9**, 1–17.
17 P. Peterson, T. E. Hayes, C. F. Arkin, E. G. Bovill, R. B. Fairweather, A. J. R. William, D. A. Triplett and J. T. Brandt, *Arch. Surg.*, 1998, **133**, 134–139.
18 S. Sinn, L. Müller, H. Drechsel, M. Wandel, H. Northoff, G. Ziemer, H. P. Wendel and F. K. Gehring, *Analyst*, 2010, **135**, 2930–2938.
19 S. Sinn, M. Eichler, L. Müller, D. Bünger, J. Groll, G. Ziemer, F. Rupp, H. Northoff, J. Geis-Gerstorfer, F. K. Gehring and H. P. Wendel, *Sensors*, 2011, **11**, 5253–5269.
20 S. Oberfrank, H. Drechsel, S. Sinn, H. Northoff and F. K. Gehring, *Sensors*, 2016, **16**, 282.
21 M. Hussain, H. Northoff and F. K. Gehring, *Talanta*, 2016, **147**, 1–7.
22 V. Efremov, R. S. Lakshmanan, J. O'Donnell and A. J. Killard, *IEEE Sens. Lett.*, 2021, **5**, 2021–2024.
23 G. Li, P. Yang, N. Huang and H. Ding, *J. Biosci. Bioeng.*, 2013, **116**, 235–245.
24 A. Kunze, C. Hesse and S. Svedhem, *Colloids Surf., B*, 2014, **116**, 446–451.
25 N. Weber, H. P. Wendel and J. Kohn, *J. Biomed. Mater. Res., Part A*, 2005, **72**, 420–427.
26 J. Fatisson, S. Mansouri, D. Yacoub, Y. Merhi and M. Tabrizian, *J. R. Soc., Interface*, 2011, **8**, 988–997.
27 A. Oseev, N. Mukhin, C. Elie-Caille, W. Boireau, R. Lucklum, T. Lecompte, F. Remy-Martin, J. F. Manceau, F. Chollet and T. Leblois, *Nanomaterials*, 2020, **10**, 1–15.
28 M. J. Santos-Martinez, I. Inkielewicz-Stepniak, C. Medina, K. Rahme, D. Arcy, D. Fox, J. D. Holmes, H. Zhang and M. W. Radomski, *Int. J. Nanomed.*, 2012, **7**, 243–255.
29 G. Sauerbrey, *Z. Phys.*, 1959, **155**, 206–222.
30 K. K. Kanazawa and J. G. Gordon, *Anal. Chem.*, 1985, **57**, 1770–1771.
31 A. Saftics, G. A. Prósz, B. Türk, B. Peter, S. Kurunczi and R. Horvath, *Sci. Rep.*, 2018, **8**, 1–14.
32 D. Johannsmann, in *Piezoelectric Sensors*, ed. C. Steinem and A. Janshoff, Springer Berlin Heidelberg, Berlin, Heidelberg, 2007, pp. 49–109.
33 T. Zhou, K. A. Marx, M. Warren, H. Schulze and S. J. Braunhut, *Biotechnol. Prog.*, 2000, **16**, 268–277.
34 K. A. Marx, *Biomacromolecules*, 2003, **4**, 1099–1120.
35 P. F. Van der Meer and D. de Korte, *Transfus. Apher. Sci.*, 2011, **44**, 297–304.
36 A. Schlagenhauf, N. Kozma, B. Leschnik, T. Wagner and W. Muntean, *Transfusion*, 2012, **52**, 1253–1259.
37 F. Bertolini and S. Murphy, *Transfusion*, 1996, **36**, 128–132.
38 G. Vit, H. Klüter and P. Wuchter, *J. Lab. Med.*, 2020, **44**, 285–293.
39 P. A. Lieberzeit, G. Glanznig, M. Jenik, S. Gazda-Miarecka, F. L. Dickert and A. Leidl, *Sensors*, 2005, **5**, 509–518.
40 D. Lavogina, H. Lust, M. J. Tahk, T. Laasfeld, H. Vellama, N. Nasirova, M. Vardja, K. L. Eskla, A. Salumets, A. Rinken and J. Jaal, *Biosensors*, 2022, **12**, 196.
41 S. Kanagaraja, I. Lundstrom, H. Nygren and P. Tengvall, *Biomaterials*, 1996, **17**, 2225–2232.
42 L.-C. Xu, J. W. Bauer and C. A. Siedlecki, *Colloids Surf., B*, 2014, **124**, 49–68.
43 O. Garraud, H. Hamzeh-Cognasse, E. Chalayer, A. C. Duchez, B. Tardy, P. Oriol, A. Haddad, D. Guyotat and F. Cognasse, *Transfus. Clin. Biol.*, 2023, **30**, 147–165.
44 X. Huang, Q. Bai, J. Hu and D. Hou, *Sensors*, 2017, **17**, 1785.
45 U. Latif, A. Mujahid, A. Afzal, R. Sikorski, P. A. Lieberzeit and F. L. Dickert, *Anal. Bioanal. Chem.*, 2011, **400**, 2507–2515.
46 H. Kilkson, S. Holme and S. Murphy, *Blood*, 1984, **64**, 406–414.
47 A. A. Anosov, E. Y. Smirnova, E. A. Korepanova and I. M. Shogenov, *Chem. Phys. Lipids*, 2019, **218**, 10–15.